coatings

MDPI

Article

Construction of Flower-like $FeCo_2O_4$ Nanosheets on Ni Foam as Efficient Electrocatalyst for Oxygen Evolution Reaction

Lijuan Zhang *, Zhonggui Quan, Yan Wang, Hangyang Li and Xu Yang

School of Materials and Chemical Engineering, Xi'an Technological University, Xi'an 710021, China; moon51102@163.com (Z.Q.); ylzln0909@163.com (Y.W.); 5191995132@163.com (H.L.); 18149120871@163.com (X.Y.)
* Correspondence: zhanglijuan0104@163.com

Abstract: Developing efficient transition metal oxide electrodes is essential to energy conversion and storage. In this work, flower-Like $FeCo_2O_4$ nanosheets supported on Ni foam were synthesized by facile hydrothermal and calcination treatment. Various temperatures influence the morphologies and oxygen evolution reaction activities. Especially, $FeCo_2O_4$/NF-120 °C catalysts showed the best oxygen evolution reaction (OER) activity due to the fact that 3D Ni foam provided good conductive substrate-forming $FeCo_2O_4$ nanosheets, which enhanced the electrochemical stability and facilitated the transport of electrolyte and release of oxygen. In addition, the synergistic effect between Fe and Co also enhanced active sites and promoted the OER catalytic performance. The flower-like $FeCo_2O_4$/Ni electrodes showed a low overpotential of 124 and 339 mV at the current density of 10 and 50 mA cm^{-2} for OER, respectively. Also, they displayed a low tafel slope of 43.78 mV dec^{-1} and good stability in alkaline electrolyte. This research could promote the design of low-cost electrocatalysts for OER.

Keywords: flower-like $FeCo_2O_4$; Ni foam; oxygen evolution reaction; electrocatalysts

check for updates

Citation: Zhang, L.; Quan, Z.; Wang, Y.; Li, H.; Yang, X. Construction of Flower-like $FeCo_2O_4$ Nanosheets on Ni Foam as Efficient Electrocatalyst for Oxygen Evolution Reaction. *Coatings* **2023**, *13*, 1875. https://doi.org/10.3390/coatings13111875

Academic Editor: Dimitrios Tasis

Received: 27 September 2023
Revised: 26 October 2023
Accepted: 30 October 2023
Published: 31 October 2023

1. Introduction

Currently, the excessive consumption of fossil fuels and severe environmental pollution are becoming urgent. It is necessary to explore renewable clean energy resources for future development. Water splitting has been widely studied to generate hydrogen energy. It includes two reactions: the hydrogen evolution reaction (HER) and the oxygen evolution reaction (OER). However, the main challenge of water splitting is due to its four-electron transfer process with additional overpotential for the OER [1,2]. Therefore, an efficient electrocatalyst with low overpotential and long-time stability is necessary. IrO_2 and RuO_2 have been considered to be the most efficient OER electrocatalysts [3]. However, because of high prices, scarcity, and inferior durability, the noble metals have limited their further wide practical applications. Therefore, it is desirable to develop low-cost and high-OER performance catalysts with improved stability.

Transition metal oxides have been studied in energy conversion and storage. Mixed transition oxide-based cobalt, especially with bimetallic spinel type structures such as $NiCo_2O_4$, $ZnCo_2O_4$, and $MnCo_2O_4$, has been widely explored because of its environmental friendliness, low cost, good structure stability, and synergistic effects [4–6]. Among the spinel type of bimetal oxides, $FeCo_2O_4$ has attracted more attention in the presence of cations with variable valence states of Fe^{2+} and Fe^{3+} in the oxidation-reduction reaction and its surface structure morphology [7]. For instance, Liu synthesized $FeCo_2O_4$ nanoparticle catalysts with an overpotential of 280 mV at 10 mA cm^{-2} [8]. However, the catalysts suffered from low electrical conductivity and poor cycle stability. In order to improve the OER electrocatalytic performance and cycle stability, many groups synthesized spinel oxide composites with conducting substrate to assure fast electron transport in electrochemical reactions [9]. For instance, Yan reported the $FeCo_2O_4$ growing on hollow graphene spheres, which exhibited better electrochemical performance than that of RuO_2/C [10]. Zhao reported $FeCo_2O_4$@$FeCo_2S_4$@PPy catalysts through a three-step electrochemical preparation,

which exhibited an excellent electrocatalytic performance with an overpotential of 280 mV for OER at 10 mA cm^{-2} [11]. Even more, the morphology of $FeCo_2O_4$ could influence the electrochemical performance. Some researchers have proven that nanosheets of catalysts often improve their electrochemical activity. Wang fabricated NiMn LDH nanosheets growing on $FeCo_2O_4$ nanoflakes. These nanoflake structures could provide a platform for NiMn LDH nanosheets, leading to an enhanced active surface area and transfer mass/charge [12]. Chao's group designed $FeCo_2O_4$ nanosheets as electrodes for H_2 production. The $FeCo_2O_4$ nanosheets had a large active surface, which may provide enough space for electrolyte ions to improve their electrochemical performances [13]. Therefore, $FeCo_2O_4$ nanosheets are expected to be a promising catalyst.

Nickel foam (NF) has been widely used as a substrate with good conductivity and a large surface area with multiple levels of porosity, which provide sufficient spaces to build up nanomaterial on it, and it is expected to enhance the conductivity of the electrode material [14]. Therefore, $FeCo_2O_4$ grown in situ on NF can avoid the falling problem of active material, which is caused by O_2 bubbles dissipating during OER reactions.

Herein, we synthesized flower-like $FeCo_2O_4$ electrode materials on NF through a simple hydrothermal and calcination method. The $FeCo_2O_4$/NF is studied through the influence of various temperatures on the structure, morphology, and surface properties, which have been associated with the electrochemical behavior of OER. Their electrochemical performances for OER were studied in 1 M KOH alkaline electrolyte. The large surface area of $FeCo_2O_4$ with flower-like structure could expose more active sites which facilitate mass and electron transfers, exhibiting low overpotential of 124 mV and 339 mV at the current density of 10 mA cm^{-2} and 50 mA cm^{-2}, respectively. In addition, the $FeCo_2O_4$/NF electrode demonstrates long cycling stability in alkaline electrolyte.

2. Materials and Methods

A piece of nickel foam (NF) was firstly cut into 1cm × 1cm, then ultrasonic cleaning with HCl solution (3 M) was performed for 0.5 h to remove the impurity on the surface. Then, the NF was washed with distilled water several times, until the solution's pH was 7. Lastly, it was put into the oven for drying.

2.1. Synthesis of $FeCo_2O_4$ /NF Composite

The $FeCo_2O_4$/NF composite was prepared by a simple hydrothermal method in a typical preparation through the following process: 1 mmol of $Fe(NO_3)_3$, 2 mmol of $Co(NO_3)_2$, 10 mmol of urea, and 6 mmol of NH_4F were dissolved in the 80 mL of distilled water and stirred for 1 h. Then, the resultant solution was transferred into the PTFE in a stainless steel autoclave and the NF was put vertically immersed into the above solution and left for 12 h. The autoclave was kept in an oven at 100, 120, 140, and 160 °C for 12 h. The $FeCo_2O_4$ NF composites were titled as $FeCo_2O_4$/NF-100, $FeCo_2O_4$/NF-120, $FeCo_2O_4$/NF-140, and $FeCo_2O_4$/NF-160, respectively. After the reaction, the suspension cooled down to room temperature. Then, the precursor was washed several times with deionized water and dried in air. Finally, the precursor was treated at 350 °C in air for 2 h. The average mass of $FeCo_2O_4$ grown on NF was about 1.8 mg/cm^2.

2.2. Characterization

The crystal structures of the samples were investigated by X-ray diffraction (XRD) with Cu-Kα radiation. The surface morphology and microstructure were obtained using a field emission scanning electron microscope (SEM, JEOL JSM-6700, JEOL Ltd., Tokyo, Japan), transmission electron microscope (TEM, JEM 2100, Japan Electronic Materials, Hyogo, Japan), and high-resolution transmission electron microscope (HR-TEM, JEM2100, JEOL, Tokyo, Japan) at 300 kV. The X-ray photoelectron spectroscopy (XPS) used monochromated Al Kα X-ray radiation (XPS, ESCALAB, 250Xi, Thermo Fisher Scientific, Waltham, MA, USA) as the source to analyze the surface chemical composition. The binding energy was

referenced with C1s peak (284.8 eV). The spectra were performed at a constant pass energy of 20 eV and steps of 0.1 eV and analyzed with a Smart-type background approach [15].

2.3. Electrochemical Measurements

The electrochemical tests were performed on a CHI 660E electrochemical workstation (CH Instruments, Inc., Shanghai, China) at room temperature in 1.0 M KOH. A standard three-electrode system with the as-prepared $FeCo_2O_4$/NF (1 cm × 1 cm) as working electrode, a graphite rod as the counter electrode, and Ag/AgCl applied as the reference electrode, respectively, was used. The applied potential was converted to the reversible hydrogen electrode (RHE) scale by the Nernst equation: Evs.RHE = Evs. Ag/AgCl + 0.098 + 0.059 pH. Linear sweep voltammograms (LSV) were performed at a scan rate of 2 mV s^{-1}. All measured LSV potentials were processed with iR-compensation. CV with the potential range 0~0.05 V (vs. Ag/AgCl) of the non-faradaic region at different scan rates of 20, 40, 60, 80, and 100 mV s^{-1} was used to assess the double layer capacitance (C_{dl}). Electric impedance spectroscopy (EIS) was performed in the potentiostatic mode with frequency from 10^5 to 0.01 Hz, and the signal amplitude of EIS was 5 mV.

3. Results

The XRD analysis of different hydrothermal temperatures of FeCo2O4/NF composites are shown in Figure 1. In order to avoid the influence of the substrate, we peeled off the powders from the Ni foam. All the powders which showed the diffraction peak at 2θ = 31.24°, 36.96°, 38.43°, 55.60°, 59.17°, 65.18° can be well identified as (220), (311), (400), (511), and (440) planes of $FeCo_2O_4$ (PDF 22-1086), respectively. Furthermore, when the temperature was at 140 and 160 °C, two weak diffraction peaks of (311) and (400) were attributed to the Fe_3O_4 phase (JCPDS no.88-0315), indicating the amount of Fe_3O_4 which coexisted in the $FeCo_2O_4$ structure [16].

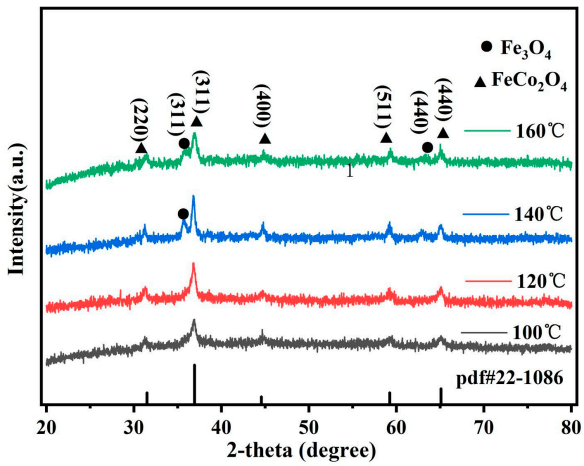

Figure 1. The XRD pattern of products with various hydrothermal temperatures.

The effects of hydrothermal temperature on the morphologies of $FeCo_2O_4$ electrodes were investigated by SEM and TEM. It can be seen in Figure 2 that the amount of urchin-like nanowires grew aggregately distributed on the surface of NF at 100 °C (Figure 2a). As the temperature increased to 120 °C, the morphology of the $FeCo_2O_4$ electrode surface changed greatly, and flower-like microspheres appeared on the surface of NF (Figure 2b). The nanosheet structure can be further observed from Figure S1, and such interconnection of nanosheets were grown vertically on the NF to form flower-like microspheres with a diameter of about 2–5 μm, which could provide a greater electrochemical active area to contact with the electrolyte and facilitate the release of O_2 during the OER [12]. In previous reports, NH_4F was very important for forming nanosheet materials [13,17]. In our experiment, it acted as a precipitant for the co-precipitation of Co^{2+} and Fe^{2+} and

as an additive to control the nanosheets of metal oxide precursors [18]. However, when the temperature further increased, $FeCo_2O_4$ nanowires appeared and wrapped $FeCo_2O_4$ nanosheets (Figure 2c), and the growth $FeCo_2O_4$ nanowires further aggregated together at the temperature of 160 °C (Figure 2d). We speculate that these morphologies would differ by their electrochemical active area, which may affect the OER activity.

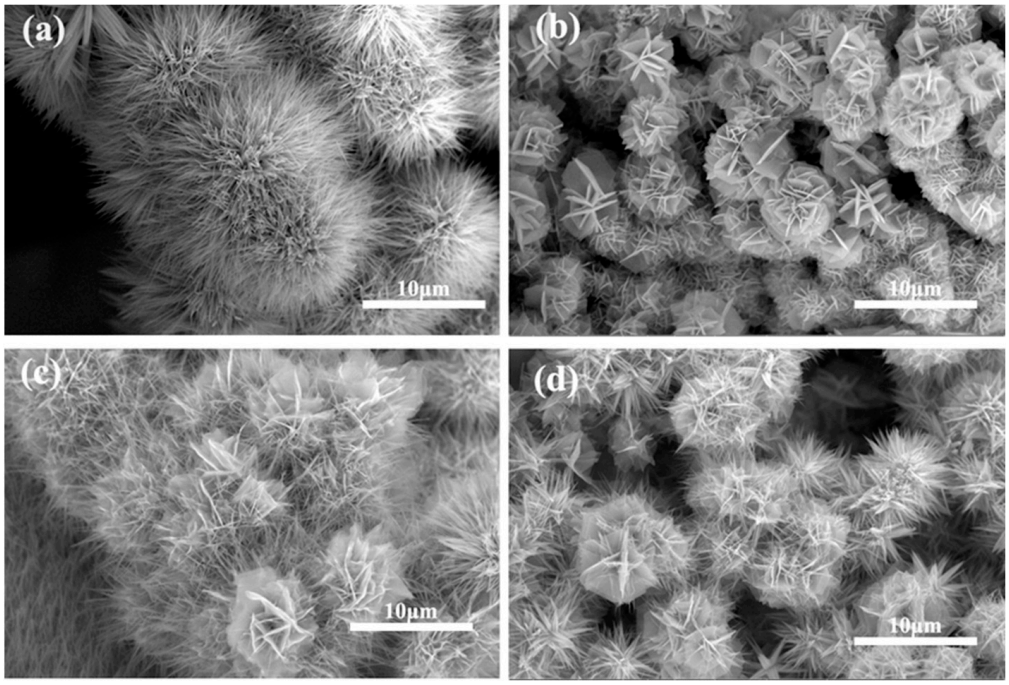

Figure 2. The SEM of products with various hydrothermal temperatures: (**a**) 100 °C, (**b**) 120 °C, (**c**) 140 °C, (**d**) 160 °C.

More morphology and structure characteristics of the composites were analyzed by TEM, and the results are shown in Figure 3. $FeCo_2O_4$/NF-120 °C displayed nanosheets with a length of about 100–200 nm (Figure 3a). Furthermore, the HR-TEM images showed lattice fringes of 0.24 nm, which corresponded to the (311) plane of $FeCo_2O_4$ (Figure 3b). The TEM image further confirmed the existence of layers of nanosheets (Figure S2). Meanwhile, the EDX spectrum (Figure S3) revealed the presence of Fe, Co, and O elements uniformly distributed on the surface of $FeCo_2O_4$/NF-120 °C (Figure 3c).

The X-ray photoelectron spectroscopy was further applied to study the surface chemical compositions of the $FeCo_2O_4$/NF-120 electrode. As shown in Figure 4, the overall survey XPS spectrum confirmed the existence of Fe, Co, and O in its respective nanosheet structures, which was in accordance with the result of EDX (Figure 4a). The high-resolution Co 2p XPS spectrum (Figure 4b) can be deconvoluted into two spin-orbit doublets along with two shake-up satellite peaks. The two doublets located at 782.5 and 797.7 eV were assigned to Co^{2+}, while the other two peaks at 780.5 and 795.2 eV can correspond to Co^{3+} [19,20]. Similarly, the deconvoluted Fe spectrum (Figure 4c) showed two main peaks at 713.2 eV and 724.5 eV, corresponding to Fe^{3+}, and the peak at 711.3 eV confirmed the presence of Fe^{2+}, with a satellite peak at 715.9 eV [21]. The high-resolution spectrum of O 1s showed three peaks, and the fitting peak of O1 at 529.6 eV was attributed to the metal-oxygen bond. The O2 located at 531.1 eV and the O3 which appeared at 533.5 eV were associated with oxygen from the hydroxyl groups and the surface-adsorbed H_2O molecule [22]. The above results reveal the co-existence of Fe^{3+}, Co^{3+}, Fe^{2+}, Co^{2+}, and O in $FeCo_2O_4$.

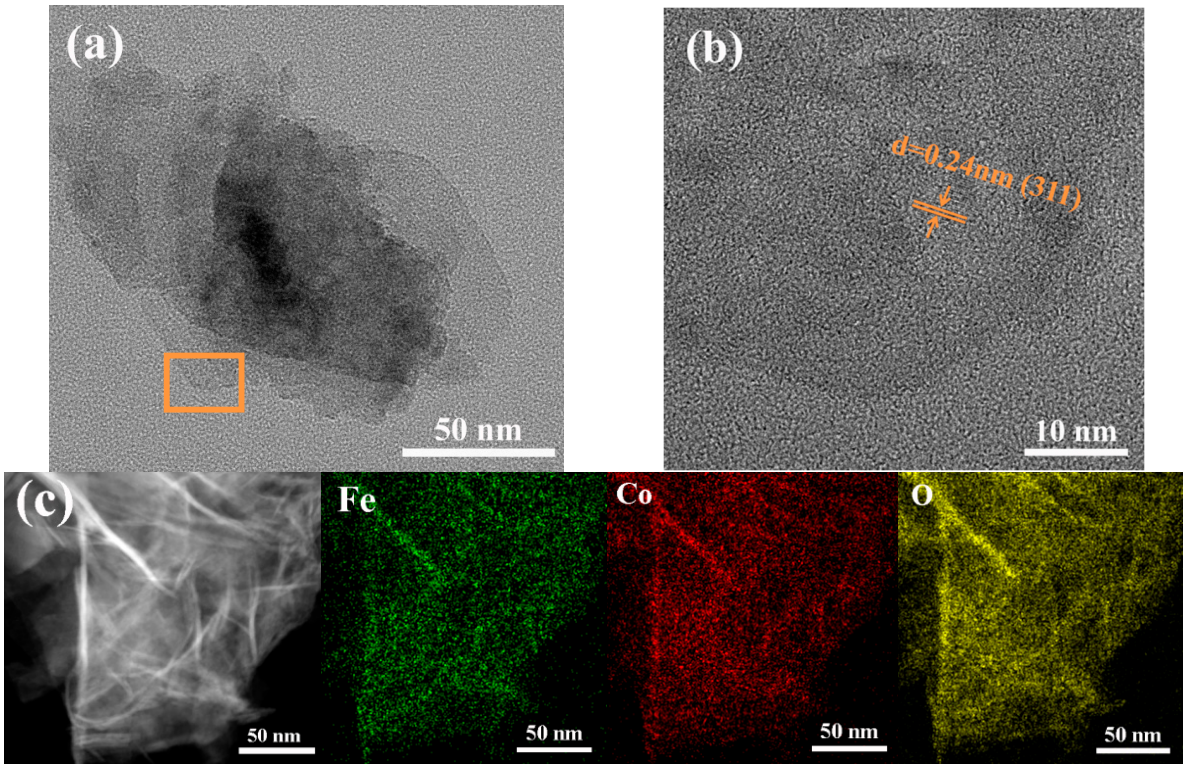

Figure 3. TEM (**a**) and HRTEM (**b**) images of $FeCo_2O_4$ nanosheets, EDS mapping of $FeCo_2O_4$ (**c**).

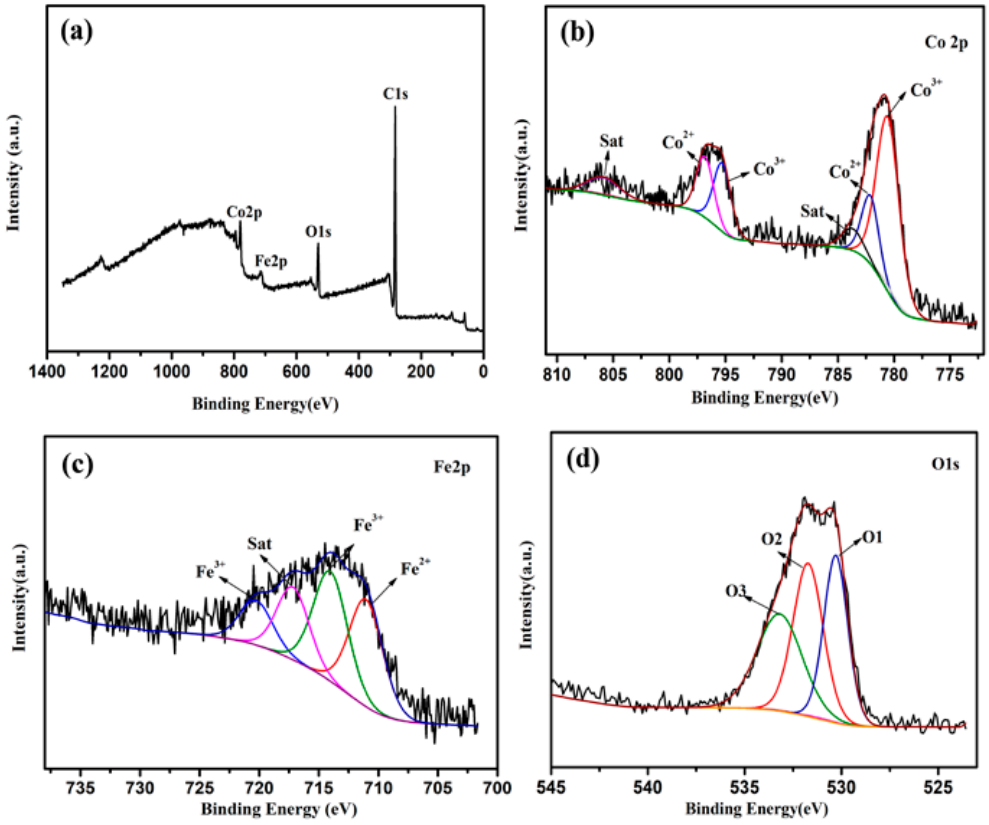

Figure 4. (**a**) XPS spectrum of $FeCo_2O_4$/NF composites. (**b**) High-resolution Co2p spectrum, (**c**) Fe2p spectrum, and (**d**) O1s spectrum.

The electrocatalytic activity of $FeCo_2O_4$/NF catalysts was evaluated by CV and linear sweep voltammetry in a 1M KOH solution (Figure S4). The cyclic voltammetry of all the electrodes exhibited a pair of reversible oxidation peak and reduction peak at about 1.42 and 1.25 V vs. RHE, respectively (Figure 5a). The nearly reversible redox peaks were ascribed to the electron (Co^{2+}–OH + OH^- → Co^{3+}–OOH + H^+ + e^-) injection into anodic and cathodic [23]. As shown in Figure 5b, $FeCo_2O_4$/NF-120 exhibited a higher current density and a lower onset potential with the applied potential than other electrodes. At the current densities of 10 mA cm^{-2}, the overpotential of $FeCo_2O_4$/NF-120 was 124 mV, which was much lower than those of $FeCo_2O_4$/NF-100 (148 mV), $FeCo_2O_4$/NF-140 (198 mV), and $FeCo_2O_4$/NF-160 (177 mV). Specifically, when the current density was increased to 50 mA cm^{-2}, the overpotential of the $FeCo_2O_4$/NF-120 was only 339 mV, which was still much lower than other temperature-prepared composites, $FeCo_2O_4$/NF-100 (405 mV), $FeCo_2O_4$/NF-140 (341 mV), and $FeCo_2O_4$/NF-160 (361 mV), as compared in Figure 5b. Furthermore, the catalytic kinetics of the electrocatalysts were also investigated by the Tafel slopes, which are shown in Figure 5c. The Tafel slope of flower-like $FeCo_2O_4$/NF-120 was 43.78 mV dec^{-1}, which was much smaller than those of the other electrocatalysts $FeCo_2O_4$/NF-100 (66.18 mV dec^{-1}), $FeCo_2O_4$/NF-140 (48.84 mV dec^{-1}), and $FeCo_2O_4$/NF-160 (57.74 mV dec^{-1}), thus confirming a superior reaction kinetics for OER. In general, a lower Tafel slope means a faster reaction kinetics [24]. Furthermore, compared with other catalysts listed in Table 1, the catalyst in our work exhibited a superior overpotential. These results strongly indicated that $FeCo_2O_4$/NF electrodes were highly efficient OER catalysts.

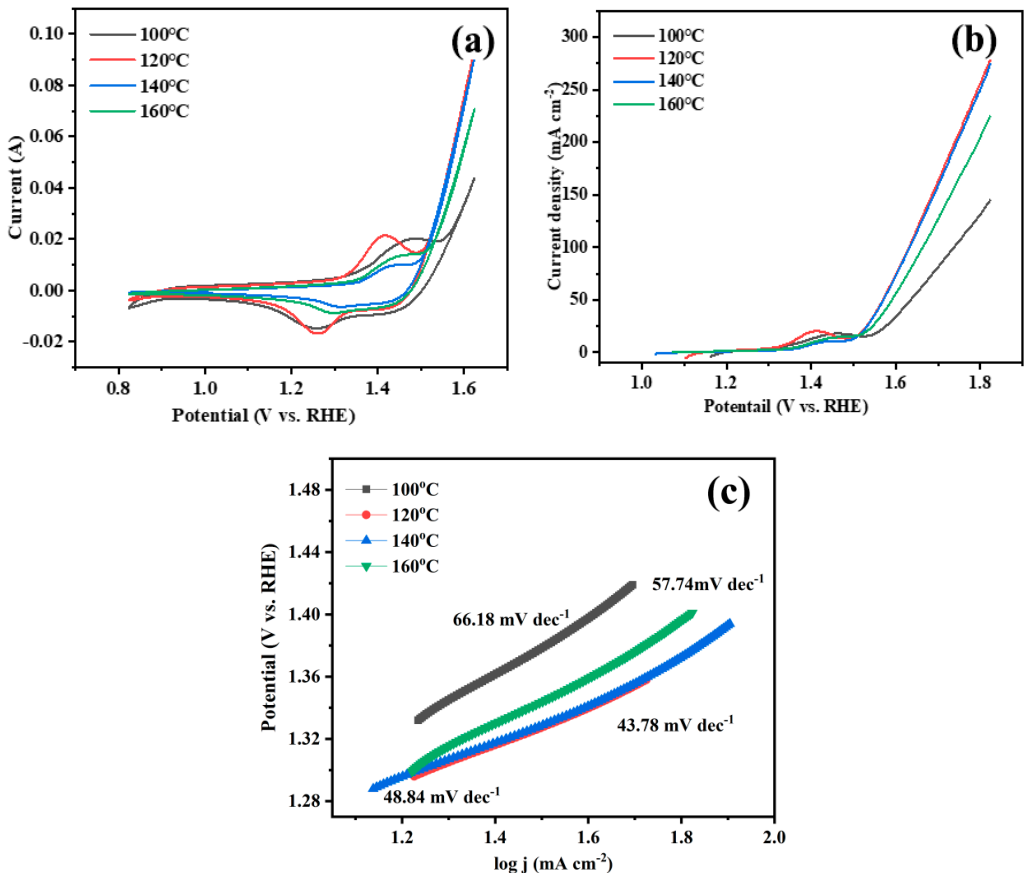

Figure 5. The electrochemical properties of $FeCo_2O_4$/NF with various hydrothermal temperatures. (**a**) CV, (**b**) LSV, (**c**) Tafel plots of the different electrodes.

Table 1. Comparison of OER catalytic performance of different catalysts.

Catalyst	Electrolyte (KOH)	Current Density (mA cm^{-2})	Overpotential for OER (mV)	References
IrO_2	1 M	50	354	[25]
NF	1 M	50	480	[26]
$FeCo_2O_4$@NPC-450	1 M	10	330	[8]
$FeCo_2O_4$@NiMn LDH	1 M	10	232	[12]
Fe-doped (Ni,Mn)Co_2O_4/NF	1 M	10	242	[27]
$FeCo_2O_4$/carbon nanofiber	6 M	10	130	[28]
$NiCo^{2+}$Fe LDH	1 M	10	290	[29]
CoFe LDH	1 M	10	319	[30]
$FeCo_2O_4$/NF-120	1 M	10 50	124 339	This work

In order to study the influence of electrode morphology on the intrinsic catalytic activity, the electrochemical active surface area (ECSA) of the OER electrocatalyst was estimated by the electrochemical double-layer capacitance (C_{dl}) [31], which was calculated by recording the cyclic voltammetry at different scan rates from 20 to 100 mV s^{-1} in a non-faradaic region. As shown in Figure 6a–d, the value of C_{dl} for the $FeCo_2O_4$NF-120 electrode was 4.41 mF $cm^{-2,}$ which was higher than those of $FeCo_2O_4$/NF-100 (2.25 mF cm^{-2}), $FeCo_2O_4$/NF-140 (0.31 mF cm^{-2}), and $FeCo_2O_4$/NF-160 (0.26 mF cm^{-2}), respectively, suggesting the nanosheets were conducive to affording large electrochemical active surface areas and exposing more active sites during the catalytic reaction, consequently promoting highly efficient OER performance [32].

Figure 7 shows the Nyquist plot of $FeCo_2O_4$/NF electrodes in a 1 M KOH electrolyte. It consists of the contact resistances (Rs) at low frequency and the charge-transfer resistance (Rct) at high frequency by equivalent circuit model. The inset shows the equivalent circuit used for fitting the Nyquist plot. The Rct of the $FeCo_2O_4$/NF-120 electrode was only 0.90 Ω, which was smaller than $FeCo_2O_4$/NF-100 (1.12 Ω), $FeCo_2O_4$/NF-140 (1.21 Ω), and $FeCo_2O_4$/NF-180 (1.63 Ω), indicating the high electric conductivity of the $FeCo_2O_4$/NF-120 electrode and the faster charge transfer kinetics and high electric conductivity during the OER [33].

In addition, the stability was also conducted with OER electrocatalysts by chronopotentiometry. As shown in Figure 8, the $FeCo_2O_4$/NF-120 electrode exhibited prominent long-term stability at 10 mA cm^{-2} in a chronopotentiometry test. The potential remained approximately constant, indicating its good stability for OER. After the cycling test, the SEM image of the $FeCo_2O_4$/NF-120 electrode is displayed in Figure S5. It shows that the catalyst still maintained a flower-like morphology, meaning that there was outstanding structural stability of $FeCo_2O_4$/NF-120.

Combining the above results, the improved OER performance of $FeCo_2O_4$/NF-120 was mainly due to the following reasons: (1) the flower-like morphology could afford a large electrochemical active surface area and expose more active sites during the catalytic reaction; (2) $FeCo_2O_4$ nanosheets grown in situ on NF could improve the conductivity and stability of the electrode. Therefore, the flower-like $FeCo_2O_4$ electrode can be used as an indication of the catalysts for OER.

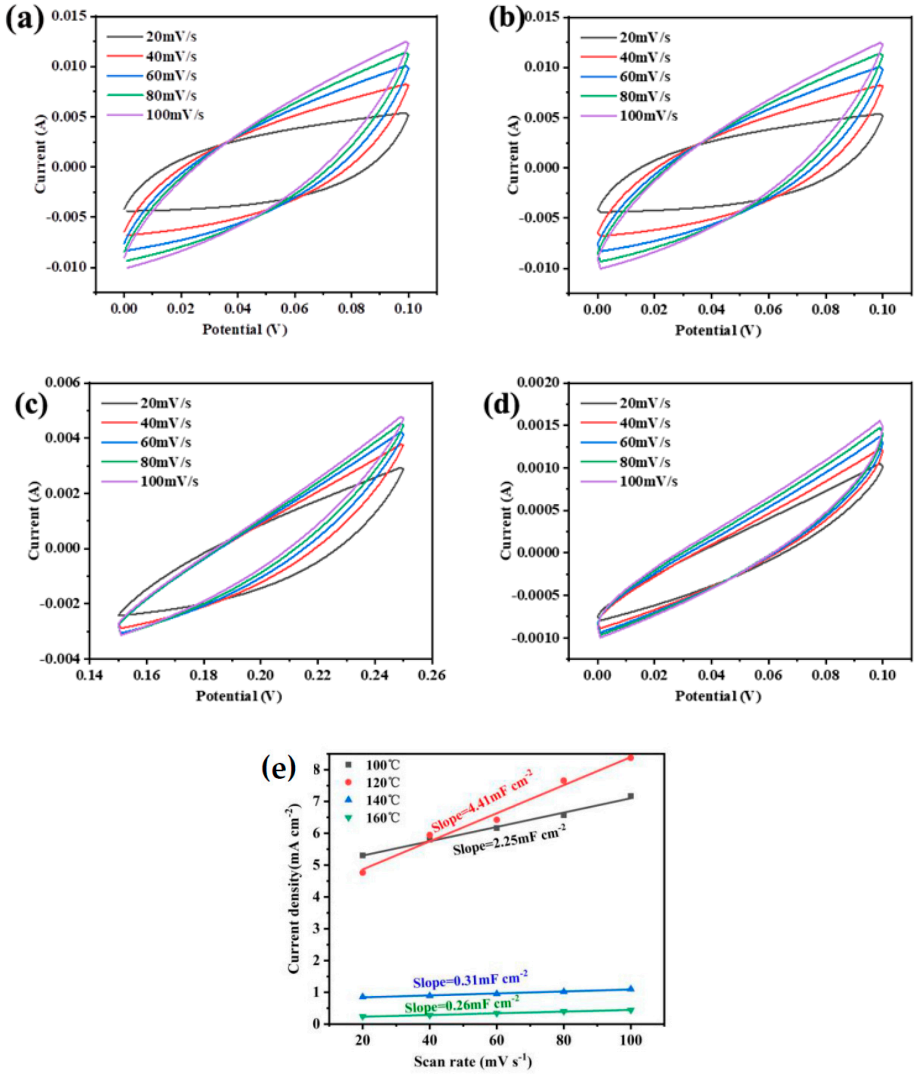

Figure 6. The CV curves and C_{dl} of $FeCo_2O_4$/NF with various hydrothermal temperatures: (**a**) 100 °C, (**b**) 120 °C, (**c**) 140 °C, and (**d**) 160 °C; (**e**) the relationship of current density and scan rate.

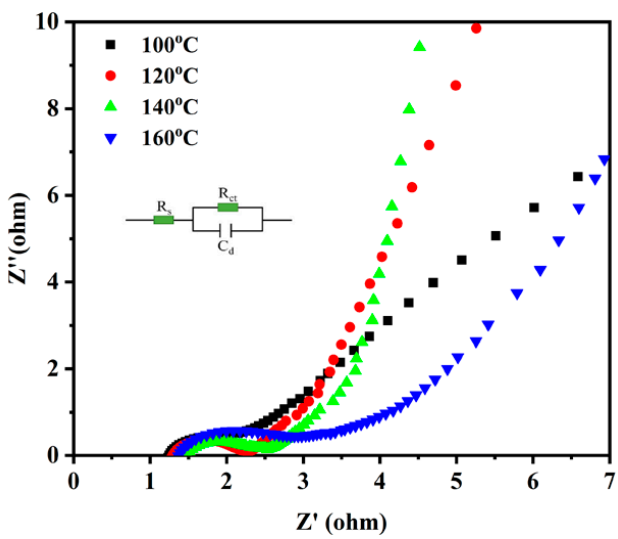

Figure 7. The electrochemical impedance spectra of the $FeCo_2O_4$/NF electrode prepared with various hydrothermal temperatures.

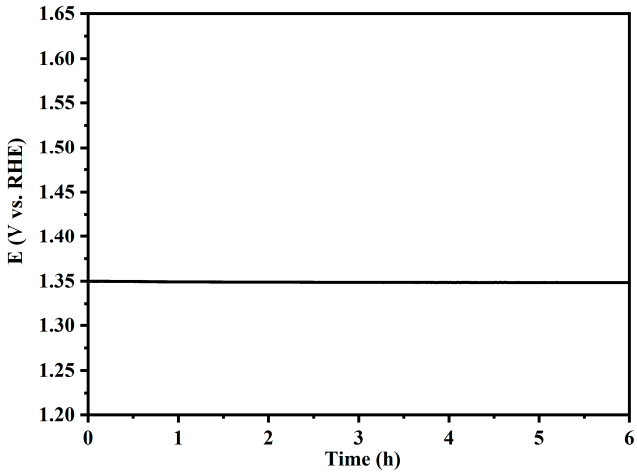

Figure 8. Chronopotentiometry curve of $FeCo_2O_4$/NF-120 electrode at a current density of 10 mA cm^{-2} in 1M KOH.

4. Conclusions

In this work, we have successfully synthesized various hydrothermal temperatures of flower-like $FeCo_2O_4$/NF nanosheets by hydrothermal and calcination processes. $FeCo_2O_4$/NF composites were used for OER catalyst in a 1 M KOH solution. Among various electrodes, $FeCo_2O_4$/NF-120 displayed the lowest on-set potential and the highest current density. The excellent performance should be attributed to the 3D macroscopic porous structure of the NF, as well as the flower-like $FeCo_2O_4$ nanosheets with porous structures, which significantly enhanced the electrochemical active area and active sites. Further, the efficient synergistic effect between Co and Fe enhanced electrocatalytic activity. Therefore, the optimized electrode $FeCo_2O_4$/NF-120 had a lower overpotential of 123 mV at 10 mA cm^{-2} and a Tafel slope of 43.78 mV dec^{-1}, as well as 6 h stable running. This work may offer a new strategy to design and explore $FeCo_2O_4$/NF electrodes for enhanced OER.

Supplementary Materials: The following supporting information can be downloaded at: https://www.mdpi.com/article/10.3390/coatings13111875/s1. Figure S1: SEM of $FeCo_2O_4$/NF-120 °C. Figure S2: TEM of $FeCo_2O_4$/NF-120 °C. Figure S3: EDX of $FeCo_2O_4$/NF-120 °C. Figure S4: LSV of $FeCo_2O_4$/NF electrodes. Figure S5: SEM of $FeCo_2O_4$/NF-120 °C after stability test.

Author Contributions: Conceptualization, L.Z. and Z.Q.; methodology, Z.Q.; software, H.L.; validation, H.L., X.Y. and Y.W.; formal analysis, L.Z.; resources, Z.Q.; investigation, Y.W.; data curation, L.Z. and Z.Q.; writing—original draft preparation, L.Z.; writing—review and editing, L.Z. and Y.W.; project administration, H.L.; visualization, X.Y.; supervision, Y.W.; funding acquisition, X.Y. All authors have read and agreed to the published version of the manuscript.

Funding: This work has been supported by the National Natural Science Foundation of China under Grant No.51521061, U1435202, and the "111" Project under Grant No. B08040. The Scientific Research Program was funded by the President's Fund of Xi'an Technological University (Project No. XAGDXJJ18008).

Institutional Review Board Statement: Not applicable.

Informed Consent Statement: Not applicable.

Data Availability Statement: Not applicable.

Conflicts of Interest: The authors declare no conflict of interest.

References

1. Gao, L.; Tang, C.; Liu, J.; He, L.; Wang, H.; Ke, Z.; Li, W.; Jiang, C.; He, D.; Cheng, L.; et al. Oxygen vacancy-induced electron density tuning of Fe_3O_4 for enhanced oxygen evolution catalysis. *Energy Environ. Mater.* **2021**, *4*, 392–398. [CrossRef]
2. Suen, N.T.; Huang, S.F.; Quan, Q.; Zhang, N.; Xu, Y.J.; Chen, H.M. Electrocatalysisi for the oxygen evolution reaction: Recent development and future perspectives. *Chem. Soc. Rev.* **2017**, *46*, 337–365. [CrossRef] [PubMed]
3. Mei, Y.J.; Feng, Y.B.; Zhang, C.X.; Qi, Q.; Hu, J. High-Entropy alloy with Mo-coordination as efficient electrocatalyst for oxygen evolution reaction. *ACS Catal.* **2022**, *12*, 10808–10817. [CrossRef]
4. Teng, Y.; Huo, Y.Q.; Li, S.T.; Niu, X.; Fan, N.; Su, Z. A zipper-like $NiCo_2O_4/Ni(OH)_2$ growing on multifunctional nickel foam with excellent capacitive performance. *J. Alloys Compd.* **2019**, *784*, 712–719. [CrossRef]
5. He, D.P.; Wang, M.Z.; Wang, X.; Feng, S.Y.; Chen, J.; Jiang, P. Construction of $ZnCo_2O_4$ nanowire arrays 3D binder-free electrode with highly catalytic activity towards glucose oxidation. *J. Solid State Chem.* **2020**, *284*, 121214. [CrossRef]
6. Lin, Y.N.; Yang, G.J.; Fu, Y.; Zhu, B.; Zhao, J.; Li, J. CoO/MnO heterostructure on three-dimensional nickel foam as efficient electrocatalyst for oxygen evolution reaction. *J. Phys. Chem. Solids* **2022**, *160*, 110373. [CrossRef]
7. Zhao, L.; Yang, D.; Ma, L.L.; Feng, X.T.; Ding, H.M. An efficient heterogeneous catalyst of $FeCo_2O_4$/g-C_3N_4 composite for catalytic peroxymonosulfate oxidation of organic pollutants under visible light. *Colloids Surf. A* **2021**, *610*, 125725. [CrossRef]
8. Liu, J.; Nan, Y.; Chang, X.X.; Li, X.Z.; Fang, Y.Y.; Liu, Y.; Tang, Y.; Wang, X.; Li, R.; Ma, J.T. Hierarchical nitrogen-enriched porous carbon materials derived from Schiff-base networks supported $FeCo_2O_4$ nanoparticles for efficient water oxidation. *Int. J. Hydrogen Energy* **2017**, *42*, 10802–10812. [CrossRef]
9. Li, S.S.; Sirisomboonchai, S.; Yoshida, A.; An, X.W.; Hao, X.G.; Abudulac, A.; Guan, G.Q. Bifunctional CoNi/$CoFe_2O_4$/Ni foam electrodes for efficient overall water splitting at a high current density. *J. Mater. Chem. A* **2018**, *6*, 19221–19230. [CrossRef]
10. Yan, W.N.; Yang, Z.R.; Bian, W.Y.; Yang, R.Z. $FeCo_2O_4$/hollow graphene spheres hybrid with enhanced electrocatalytic activities for oxygen reduction and oxygen evolution reaction. *Carbon* **2015**, *92*, 74–83. [CrossRef]
11. Zhao, D.P.; Dai, M.Z.; Zhao, Y.; Liu, H.Q.; Liu, Y.; Wu, X. Improving electrocatalytic activities of $FeCo_2O_4$@$FeCo_2S_4$@PPy electrodes by surface/interface regulation. *Nano Energy* **2020**, *72*, 104715. [CrossRef]
12. Gao, G.; Wang, K.; Wang, X.T. 2D/2D core/shell structure of $FeCo_2O_4$@NiMn LDH for efficient oxygen evolution reaction. *J. Alloys Compd.* **2023**, *937*, 168478. [CrossRef]
13. Gao, S.Q.; Fan, J.C.; Liao, H.W.; Xiao, G.C.; Li, S.D.; Cui, K.X.; Niu, C.Q.; Luo, W.B.; Chao, Z.S. Three dimensional $FeCo_2O_4$ nanosheets for integrated all-solid-state supercapacitors and electrochemical energy-saving H_2 production. *Mater. Chem. Phys.* **2022**, *287*, 126332. [CrossRef]
14. Zhang, L.J.; Yuan, H.C.; Li, X.; Wang, Y. Hydrothermal synthesis of $NiCo_2O_4$@$NiCo_2O_4$ core-shell nanostructures anchored on Ni foam for efficient oxygen evolution reactions catalysts. *Coatings* **2022**, *12*, 1240. [CrossRef]
15. Major, G.H.; Farley, N.; Sherwood, P.M.A.; Linford, M.R.; Terry, J.; Fernandez, V.; Artyushkova, K. Practical guide for curve fitting in X-ray photoelectron spectroscopy. *J. Vac. Sci. Technol. A* **2020**, *38*, 061203. [CrossRef]
16. Li, S.S.; Wang, Y.; Sun, J.L.; Xu, C.J.; Chen, H.Y. Simple preparation of porous $FeCo_2O_4$ microspheres and nanosheets for advanced asymmetric suepercapacitors. *ACS Appl. Energy Mater.* **2020**, *3*, 11307–11317. [CrossRef]
17. Wang, X.H.; Xing, J.J.; Fu, X.L. Cu-doped NiFe layered double hydroxide nanosheets on nickel foam as an effective and durable electrocatalyst for oxygen evolution reaction. *Int. J. Mod. Phys. B* **2023**, *37*, 2350260. [CrossRef]
18. Dong, F.; Liu, X.H.; Irfan, M.; Yang, L.; Li, S.L.; Ding, J.; Li, Y.; Khan, I.U.; Zhang, P.P. Macaroon-like $FeCo_2O_4$ modified activated carbon anode for enhancing power generation in direct glucose fuel cell. *Int. J. Hydrogen Energy* **2019**, *44*, 8178–8187. [CrossRef]
19. Liu, L.; Zhang, H.; Mu, Y.; Yang, J.; Wang, Y.; Yang, J.; Wang, Y. Porous Iron cobaltate nanoneedles array on nickel foam as anode materials for lithium-ion batteries with enhanced electrochemical performance. *ACS Appl. Mater. Interfaces* **2016**, *8*, 1351–1359. [CrossRef]
20. Vishnu, V.; Kumar, N.; Narayanasamy, S. Development of Fe_3O_4/CAC nanocomposite for the effective removal of contaminants of emerging concerns (Ce^{3+}) from water: An ecotoxocological assessment. *Environ. Pollut.* **2021**, *285*, 117326. [CrossRef]
21. Yamashita, T.; Hayes, P. Analysis of XPS spectra of Fe^{2+} and Fe^{3+} ions in oxide materials. *Appl. Surf. Sci.* **2008**, *254*, 2441–2449. [CrossRef]
22. Ni, L.; Zhou, J.H.; Chen, N.N.; Li, X.G.; Xu, S.C.; Zhang, L.; Lu, C.L.; Chen, J.; Xu, L.; Hou, W.H. In situ direct growth of flower-like hierarchical architecture of CoNi-layered double hydroxide on Ni foam as an efficient self-supported oxygen evolution electrocatalyst. *Int. J. Hydrogen Energy* **2020**, *45*, 22788–22796. [CrossRef]
23. Harada, M.; Kotegawa, F.; Kuwa, M. Structural changes of spinel MCo_2O_4(M=Mn, Fe, Co, Ni and Zn) electrocatalysts during the oxygen evolution reaction investigated by in stiu X-ray Adsorption spectroscopy. *ACS Appl. Energy Mater.* **2022**, *5*, 278–294. [CrossRef]
24. Zhang, J.Y.; Sun, X.; Liu, Y.; Hou, L.R.; Yuan, C.Z. Design and construction of bi-metal MOF-derived yolk-shell $Ni_2P/ZnNp_2$ hollow microspheres for efficient electrocatalytic oxygen evolution. *Mater. Chem. Front.* **2020**, *4*, 1366. [CrossRef]
25. Hu, J.M.; Zhang, J.Q.; Cao, C.N. Oxygen evolution reaction on IrO_2 based DSA type electrodes:kinetics analysis of Tafel lines and EIS. *Int. J. Hydrogen Energy* **2003**, *29*, 791–797. [CrossRef]
26. Shrestha, N.K.; Patil, S.A.; Han, J.H.; Cho, S.; Inamdar, A.I.; Kim, H.; Im, H. Chemical etching induced microporous nickel backbones decorated with metallic Fe@hydroxide nanocatalysts: An efficient and sustainable OER anode toward industrial alkaline water-splitting. *J. Mater. Chem. A* **2022**, *10*, 8989–9000. [CrossRef]

27. Shi, H.; Zha, Q.; Ni, Y. Fe-doped (Ni, Mn)Co_2O_4 nanorod arrays on Ni foam as highly efficient electrocatalyst for oxygen evolution reaction in alkaline and neutral conditions with superb long-term stability. *J. Alloys Compd.* **2022**, *904*, 164052. [CrossRef]
28. Alegre, C.; Busacca, C.; Di Blasi, A.; Di Blasi, O.; Aricò, A.S.; Antonucci, V.; Baglio, V. Toward more efficient and stable bifunctional electrocatalysts for oxygen electrodes using $FeCo_2O_4$/carbon nanofiber prepared by electrospinning. *Mater. Today Energy* **2020**, *18*, 100508. [CrossRef]
29. Chen, S.; Yu, C.; Cao, Z.F.; Huang, X.P.; Wang, S.; Zhong, H. Trimetallic NiFeCr-LDH/MoS_2 composites as novel electrocatalyst for OER. *Int. J. Hydrogen Energy* **2021**, *46*, 7037–7046. [CrossRef]
30. Hao, C.; Wu, Y.; An, Y.; Cui, B.; Lin, J.; Li, X.; Wang, D.; Jiang, M.; Cheng, Z.; Hu, S. Interface-coupling of CoFe-LDH on MXene as high-performance oxygen evolution catalyst. *Mater. Today Energy* **2019**, *12*, 453–462. [CrossRef]
31. Long, X.; Li, J.; Xiao, S.; Yan, K.Y.; Wang, Z.L.; Chen, H.N.; Yang, S.H. A strongly coupled graphene and FeNi double 372 hydroxide hybrids as an excellent electrocatalyst for the oxygen evolution reaction. *Angew. Chem. Int. Ed. Engl.* **2014**, *53*, 7584–7588. [CrossRef] [PubMed]
32. Bi, Y.; Cai, Z.; Zhou, D.; Tian, Y.; Zhang, Q.; Zhang, Q.; Kuang, Y.; Li, Y.; Sun, X.; Duan, X. Understanding the incorporating effect of Co^{2+}/Co^{3+} in NiFe-layered double hydroxide for electrocatalytic oxygen evolution reaction. *J. Catal.* **2018**, *358*, 100–107. [CrossRef]
33. Magalhães, R.S.; Bargiela, P.; Rocha, M.G.C.; Gild, E.S.; Souza, A.R. Iron Cobaltite ($FeCo_2O_4$) nanocatalysts for water-oxidation: Effects of annealing temperature on catalytic properties. *J. Braz. Chem. Soc.* **2022**, *33*, 1163–1171. [CrossRef]